19

A CFD Study of Passive Solar Shading

[1]Baxevanou C.A.*, [1]Fidaros D.K., [2]Tzachanis A.D.
[1]*Centre for Research and Technology-Thessaly, Institute of Technology and Management of Agricultural Eco-systems, Technology Park of Thessaly, 1st Industrial Area of Volos, 38500 Volos, Greece, cbaxe@cereteth.gr, dfeid@cereteth.gr*
[2]*Technological Educational Institute (TEI) of Larissa, Dept. of Mechanical Engineering, 41110 Larissa, Greece, tzach@teilar.gr*

Abstract

In the present study is investigated numerically the flow and transport phenomena in a test cell with its south side partially shaded by trailing plants and the cover shaded by a shelter. The two dimensional unsteady transport equations for the velocities, turbulence, energy and spectral intensity of radiation are solved numerically by a finite volume numerical model. The turbulent nature of the flow is simulated by the well known two equation k-ω high Re model while the incident radiation is used the Discrete Ordinates (DO) model and two wavelength bands are considered for the solar and thermal radiation. The model efficiently renders the buoyancy effects inside the cell, the cooling capacity of the plants, the heat transfer phenomena of solar radiation and heat conduction through the cell walls. The thermophysical and spectral optical properties of the involved materials were taken into account and not only the shading effect of trailing plant. The model was validated successfully via comparison with measured data that correspond in one day of August in Central Greece. A parametric study was carried out for other 4 months (May, June, July and September). The results are given in terms of fields of flow, radiation and temperature inside the test cell and in the space between this and the shading devices (shelter and trailing plants). Daily variations of average temperatures, solar radiation, air flow velocities and cooling load reduction are also given. The cooling load reduction ranges between 34 kWh/month per wall meter in September, and 63 kWh/month per wall meter in July, even without taking into account the temperature reduction due to the plants transpiration. The developed model can be used for the evaluation of various plants performance as passive solar shading configurations.

Notation

a	porous permeability [m^2]
C_2	inertial resistance factor [1/m]
C_p	specific heat capacity [J/(kg K)]
d	thickness [m]
e	specific energy (per unit mass) [J/Kg]

f_b buoyancy force [Nt/m^3]
f_d diffuse fraction of incident radiation [-]
h sensible enthalpy [J/Kg], convective heat transfer coefficient [W/m^{2}K]
G normal solar irradiation [W/m^2]
$\overline{H_b}$ monthly average daily beam irradiation [Wh/m^2]
$\overline{H_d}$ monthly average daily diffuse radiation [Wh/m^2]
$\overline{H_{tot}}$ the monthly average daily radiation [Wh/m^2]
I radiation intensity [W/m^2]
I_v radiation intensity normal to vertical plane [W/m^2]
I_h radiation intensity normal to horizontal plane [W/m^2]
I_λ radiation intensity for wavelength λ [W/(m^2 src)]
$I_{b\lambda}$ black body intensity given by the Planck function [W/m^2]
k turbulent kinetic energy [J/Kg], Thermal conductivity [W/mK]
k_{eff} effective conductivity [W/mK]
k_t turbulent thermal conductivity [W/mK]
L latitude [deg]
n refractive index of medium b [-], number of the day of a year [-]
NT total daily duration of sunlight [h]
Nu nusselt number [-] (Nu=convection/conduction) Nu=hL/K
P pressure [Pa]
r_i reflectivity of medium I [-]
$\vec{r}$ position vector [-]
R_b the ratio of beam irradiation on the plane to that on a horizontal plane [-]
S_h radiation source term [J]
$\vec{s}$ radiation direction vector [-]
t time [s]
time time since sunrise [sec]
t_s sunrise time [h]
T temperature [K]
Ta ambient temperature [K]
T_0 operating reference temperature [K]
U_i average velocity in i-direction [m/s]
x_i component in i-direction [m]

Greek Letters

α absorptivity [-]
α_λ spectral absorption coefficient [1/m] – or extinction coefficient
β Thermal expansion coefficient [1/K], the surface slope [deg]
γ the surface azimuth angle [deg]
δ declination [deg]
ε turbulent dissipation rate [J/(Kg s)], emissivity [-]
θ_a angle between the normal to the surface and the incident radiation [deg]
θ_b angle between the normal to the surface and the refracted radiation [deg]
θ_z solar zenith angle [deg]

λ wavelength [m^{-1}]
μ viscosity [Pa sec]
μ_t turbulent viscosity [Pa sec]
ρ density [kg/m^3]
ρ_0 constant flow density [kg/m^3]
σ_s scattering coefficient [1/m]
$(\tau_{ij})_{eff}$ effective stress tensor [Nt/m^2]
τ_i transmissivity of medium i [-]
Φ phase function [-]
ω specific dissipation rate [s^{-1}] , hour angle [deg]
ω_s sunrise hour angle [deg]
Ω' solid angle [deg]

1. Introduction

The placing of plants in the vicinity of the south walls of a building as solar protection system is an old and well-known technique in traditional architecture and a basic parameter in bioclimatic design, especially for countries with a climate characterized by long hot days in the summers. Plants offer the potential of solar control in buildings as well as of passive cooling. Deciduous plants can reduce excessive solar heat gains during the summer allowing the solar light to reach the building's interior during the summer. This way they contribute in reduction of air conditioning devices usage during the periods of peak power demand (Achard, P. & Gicquel, R., 1986; Goulding, J. R. et al., 1993). It has been proved that by adding one tree the cooling energy savings can vary in the range of 12-24%. Three trees per house could reduce the cooling load from 17% to 57% (Akbari, H. et al., 1997; Raeissi, S. & Taheri, M., 1999). Plants can achieve this reduction operating in two ways: a) operating as natural shading and b) reducing the air temperature through transpiration. Plants not only improve the building's energy performance during summer but they also affect appearance of them as they can be incorporated in the architectural design offering an acceptable and aesthetical result (Carter, C. & De Villiers, J., 1987; Goulding, J. R. et al., 1992).
In the present study a numerical model is developed in order to study the transport phenomena in a test cell with its south façade partially shaded by trailing deciduous plant called *Parthenocissus quinquefoliant*. It is taken into account the plants' shading effect taking account their optical properties and their ability of heating storage but not the transpiration. The numerical model will be validated against existed measurements. Then a parametric numerical study will allow the systematic quantification of the energy gains which could establish a new way of thinking for passive cooling design.

2. Literature review

Until now the majority of studies about plants as passive solar devices, concerned the experimental investigation of the energy saving and alteration of the building internal microclimate offered by the plants' shadow.
According to measurements in two houses (Akbari, H., Kurn, D. M. et al., 1997) the cooling energy saving yielded by trees appearance can reach levels up to 30% corresponding to daily savings of 3.6 to 4.8 kWh/d. Experimental investigation of shading with trees,

positioned around buildings - especially on the southern side (Papadakis, G. et al., 2001) have also been performed. The results have shown that trees constitute an excellent passive cooling system, being able to reduce the peak solar heat gain from 600 W/m^2 to 180 W/m^2, even with measured temperatures in the sunlit and in the shaded area of about 42^{o}C and 33^{o}C respectively.
Another group of studies developed analytical models which usually have been incorporated in software. In the paper (Tzachanis, A. D. & Sdravopoulou, C., 2002) the periodic steady heat gain in buildings is simulated with a dynamic model. In the work (Liu, Y. & Harris, D. J., 2008) an energy software package, the ESP-r, was used in order to study the effect of trees sited in the north of a house, in the heating-energy consumption.
Recently numerical methods are used for the study of heat transfer mainly in solar chimneys (Gan, G., 2006; Miyazaki, T. et al., 2006) used in the south facades. Numerical methods are more widely used for study of the microclimate developed in urban street canyons (Erell, E. & T. Williamson, 2006; Ali-Toudert, F. & Mayer, H., 2007).
As far it concerns numerical studies for the use of plants as passive solar systems there are some hybrid approaches like the one presented in (Mochida, A. et al., 2006) where a CFD model is used for the study of convective and radiative heat transports phenomena around buildings and the program 'TRNSYS' for the heat load calculations inside them.
In the numerical study (Baxevanou, C. A. et al., 2008) the test cell of present study was investigated considering the plants only as a shading device without taking into account exact optical and thermal properties and the temporal heat storage. Nevertheless this preliminary work was the starting point for the numerical model presented here.

3. Physical problem

In the present study the flow and transport phenomena inside and around a test cell with its south side shaded by trailing plant is investigated numerically. The physical model is an experimental setup of a cubic shaped test cell having a volume of approximately 30m^3 build at the TEI of Larissa, Greece (Tzachanis, A. D., 2008). This set-up gives the possibility to carry out experiments "in situ" with the instrumentation and the data acquisition system being placed inside the cell and is presented in Fig.1. Its south face is shaded by trailing plant called *Parthenocissus quinquefoliant*. The test cell walls are fabricated by a 5 cm sandwich material consisting of a 4.8 cm polyurethane layer with steel claddings. The whole construction was placed on a steel frame with wheels enabling easily the orientation change of the cell. Over the ceiling there is an inclined shelter of the same material that allows the cell cooling by convection from the air circulating between the ceiling and the shelter.

Fig. 1. A front view of the passive solar system

3.1 Geometry

In the following Fig.2 the geometry of a test cell cross-section is presented.

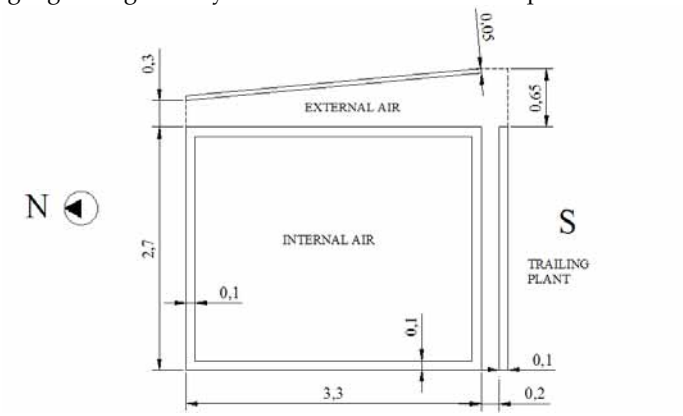

Fig. 2. Cross-section geometry

3.2 Properties

In the following tables the thermophysical and spectral optical properties of the involved materials are given. As it is said the walls are sandwich of polyurethane and steel cladding painted white. In this simulation is considered as a homogenous material with the effective properties given in the following Table 1. The plants' optical properties correspond to

tomato crop according to (Zhang, Y. et al., 1997) and they are radiation wave length depended. They are given for two spectral bands, the first is considered as solar band and corresponds to wavelength λ=0-1.1 μm and the second is considered as thermal band and corresponds to wavelength λ=1.1–100 μm. The trailing plants are modelled as porous medium where the 40% of the total volume is air. The air is considered to contain enough vapors to present noticeable absorptivity (Modest, M. F., 2003).

Property	Air	Plant		Walls
		λ=0-1.1	λ=1.1-100	
Density, ρ [Kg/m³]	1.225	700		807
Specific Heat Capacity, Cp, [J/KgK]	1006.43	2310		465
Conductivity, k [W/m]	0.0242	0.173		0.0255
Viscosity, μ [Pasec]	1.789×10^{-5}	-		-
Thermal expansion coefficient, β [1/K]	0.00343	-		-
Absorptivity, α	0.19	0.71	0.95	0.85
Refractive index, n	1	2.69	1.22	24.62
Emissivity, ε	0.05	0.59		0.45
Transmissivity, τ	0.81	0.08	0	0

Table 1. Material properties

4. Mathematical model

In this work we study the flow and the transport phenomena developed in the air inside the test cell, the air between the test cell and the shading devices (shelter and trailing plants) and the solid materials involved (test cell walls, shelter and trailing plants). The flow is assumed to be 2D, incompressible, unsteady and turbulent since those phenomena are studied along the symmetry cross-section in the North-South plane as shown in Fig.2. This simplification is adopted in this study in order to save computational effort although the aspect ratio of the sides is rather small. The flow and transport phenomena for air flow and heat and radiation transfer are described by the Navier-Stokes equations (Ferziger, J. H. & Perić, M., 2002).

4.1 Transport equations

The time-averaged Navier-Stokes equations, for the mass and momentum transport are given as follow (Launder, B. E. & Spalding, D. B., 1974):

Continuity equation

$$\frac{\partial U_i}{\partial x_i} = 0 \tag{1}$$

Momentum conservation

$$\rho\left(\frac{\partial U_i}{\partial t} + U_j \frac{\partial U_i}{x_j}\right) = -\frac{\partial P}{\partial x_j} + \frac{\partial}{\partial x_j}\left[\left(\mu + \mu_t\right)\frac{\partial U_i}{\partial x_j}\right] + f_b + S_i \tag{2}$$

Where, U_i the time averaged i-direction velocity, ρ the density, P the pressure, μ the viscosity, μ_t the turbulent viscosity, f_b the buoyancy force, t the time and S_i source term

expressing the pressure drop across the plants which are considered to be porous medium.

4.2. Boussinesq approximation

The density variation is calculated according to the Boussinesq model in order to take into account the natural convection effects. The use of Boussinesq model offers faster convergence, than considering the density variable in all equations. In this model the density is a constant value in all solved equations except from the buoyancy term calculation in the momentum equation:

$$f_b = (\rho - \rho_0) g \approx -\rho_0 \beta (T - T_0) g \tag{3}$$

This way the ρ is eliminated from the buoyancy term using the Boussinesq approximation:

$$\rho = \rho_0 (1 - \beta \Delta T) \tag{4}$$

Where β is the thermal expansion coefficient, T the temperature, ρ_o and T_o the corresponding reference values for density and temperature and g the gravity acceleration.

4.3 Porous media Treatment

The trailing plants, which are a shading device, are simulated as porous media adding a momentum source term S_i to the Navier-Stokes fluid flow equation. This term express the pressure drop caused in the flow by their presence and it is composed by a viscous loss term known as Darcy law and an inertial loss term, according to the following:

$$S_i = -\left(\frac{\mu}{\alpha} u_i + C_2 \rho u_i^2 \right) \tag{5}$$

where, a is the porous permeability and C_2 the inertial resistance factor.

4.4 Energy Treatment

Energy Conservation is described by the following equation

$$\rho \left(\frac{\partial h}{\partial t} + U_i \frac{\partial h}{\partial x_i} \right) = k_{eff} \frac{\partial}{\partial x_i} \left(\frac{\partial T}{\partial x_i} \right) + S_h \tag{6}$$

Where ε is specific energy (per unit mass), k_{eff} the effective conductivity, $(\tau_{ij})_{eff}$ the effective stress tensor and S_h source term which add the radiation contribution to the energy conservation equation. Auxiliary relationships for the calculations of quantities appeared in energy equation are presented here. Specifically relationships are given for the calculation of effective and turbulent conductivity as well as for the energy and enthalpy.
Effective Conductivity

$$k_{eff} = \gamma k_{feff} + (1 - \gamma) k_s \tag{7}$$

Where γ is the porosity, when γ=1 there is only fluid, k_{feff} the fluid effective conductivity and k_s the solid conductivity. The fluid effective thermal conductivity is given by

$$k_{feff} = k_f + k_t \tag{8}$$

Where k_f is the fluid conductivity and k_t the turbulent conductivity given by
Turbulent Conductivity

$$k_t = \frac{C_p \mu_t}{\mathrm{Pr}_t} \tag{9}$$

Where, C_p is the specific heat capacity and Pr_t the turbulent Prandtl number while the enthalpy h is given by the equation

$$h = \int_{T_0}^{T} C_p dT \tag{10}$$

The calculation of the energy equation source term is important because incorporates the effect of radiation in the energy balance and it is taken from the solution of the radiative transport equation. When the velocity takes null value, as it happens in solid materials, the above equation is decreased in the equation of conductivity for heat transfer.

$$\rho \frac{\partial T}{\partial t} + k_s \frac{\partial^2 T}{\partial x_i^2} + S_h = 0 \tag{11}$$

4.5. Turbulent model

The flow in both internal and external air is turbulent. The effect of turbulence is implemented via the high Re k-ω model of Wilcox [21](Wilcox, D. C., 1998).
Turbulent kinetic energy, k, transport equation is given by

$$\rho \frac{\partial k}{\partial t} + \rho U_j \frac{\partial k}{\partial x_j} = \tau_{ij} \frac{\partial U_i}{\partial x_j} - \beta^* \rho k \omega + \frac{\partial}{\partial x_j}\left[\left(\mu + \mu_t \sigma^* \right) \frac{\partial k}{\partial x_j} \right] \tag{12}$$

Where, ω is the specific dissipation rate, for which the transport equation is

$$\rho \frac{\partial \omega}{\partial t} + \rho U_j \frac{\partial \omega}{\partial x_j} = \alpha \frac{\omega}{k} \tau_{ij} \frac{\partial U_i}{\partial x_j} - \beta \rho \omega^2 + \frac{\partial}{\partial x_j}\left[\left(\mu + \mu_\tau \sigma \right) \frac{\partial \omega}{\partial x_j} \right] \tag{13}$$

with $\omega = \frac{\varepsilon}{\beta^* k}$, $\mu_\tau = \frac{k\rho}{\omega}$, α=5/9, β=3/40, β*=9/100, σ=1/2 and σ*=1/2, where ε is the turbulence dissipation rate.

4.6. Radiation model

In order to simulate the effect of solar incident radiation on the trailing plants, the shelter and the test cell walls, the Discrete Ordinates (DO) model is used. In this model it is assumed that radiation energy is 'convected' through the medium at its own speed simultaneously in all directions. The DO model allows the solution of radiation at semi-transparent walls. It can be used to non-gray radiation using a gray-band model. So it is adequate for use with participating media with a spectral absorption coefficient α_λ that varies in a stepwise fashion across spectral bands. The DO radiation model solves the Radiative Transfer Equation (RTE) for a finite number of discrete solid angles, each associated with a vector direction $\vec{s}$ fixed in the global Cartesian system (x,y,z). It transforms the RTE equation into a transport equation for radiation intensity in the spatial coordinates (x,y,z). The DO model solves for as many transport equations as there are directions $\vec{s}$ (Raithby, G. D. & Chui, E. H., 1990; Chui, E. H. & Raithby, G. D., 1993). The RTE for spectral intensity $I_\lambda(\vec{r},\vec{s})$ turns to

$$\nabla\left(I_\lambda(\vec{r},\vec{s})\vec{s}\right) + \left(a_\lambda + \sigma_s\right) I_\lambda(\vec{r},\vec{s}) = a_\lambda n^2 I_{b\lambda}(\vec{r}) + \frac{\sigma_s}{4\pi} \int_0^{4\pi} I_\lambda(\vec{r},\vec{s}') \Phi(\vec{s}\cdot\vec{s}) d\Omega \tag{14}$$

In this equation the refractive index, the scattering coefficient and phase function are assumed independent of wavelength. The phase function Φ, is considered isotropic. The angular space 4π at any spatial location is discritized into $N_\theta x N_\varphi$ solid angles of extent ω_i, called control angles. The angles θ and φ are the polar and azimuthal angles, and are measured with respect to the global Cartesian system (x,y,z). In our case a 3x3 pixilation is used. Although in this equation the refraction index is taken constant, in the calculation of black body emission as well as in the calculation of boundary conditions imposed by semi-transparent walls the band length depended values of refractive index are used. This angular discretization provides us with a moderate computational cost but it may introduce discretization errors at boundaries when the solid angles are bisected by them (Raithby, G. D., 1999). Solving a problem with a fine angular discretization is very CPU-intensive. The RTE equation is integrated over each wavelength. Then the total intensity $I(\vec{r},\vec{s})$ in each direction $\vec{s}$ at position $\vec{r}$ is computed using

$$I(\vec{r},\vec{s}) = \sum_{\kappa} I_{\lambda_\kappa}(\vec{r},\vec{s})\Delta\lambda_\kappa \tag{15}$$

Where, the summation is over the wavelength bands. The RTE equation is coupled with the energy equation through a volumetric source term given by the following equation (Kim, S. H. & Huh, K. Y., 2000):

$$S_h = -\frac{\partial q_{r_i}}{\partial x_i} = a_\lambda\left(4\pi I_{b\lambda}(\vec{r}) - \int_{4\pi} I(\vec{r},\vec{s})\,d\Omega\right) \tag{16}$$

The spectral absorption coefficient, α_λ is computed from the absortpivity, α, according to the media thickness, d:

$$\alpha_\lambda = \frac{1}{d}\ln\left(\frac{1}{1-\alpha}\right) \tag{17}$$

5. Numerical model

The problem is simulated through 2D transport equations for mass, momentum, turbulence, energy and spectral radiation. Those transport equations (1, 2, 6, 12, 13 and 14) are solved numerically using the finite volume method.

5.1 Grid geometry

For the simulation is used a structured collocated grid consisted of 18864 cells as shown in the following Fig.3. The internal air field is consisted of 12400 cells. The external air field is consisted of 3744 cells. The plants are considered porous media consisted of 432 cells. The transport equations are also solved inside the solid walls which are discretized to 4 series and inside the shelter which is discretized to 3 series of cells resulting to 2288 cells in total.

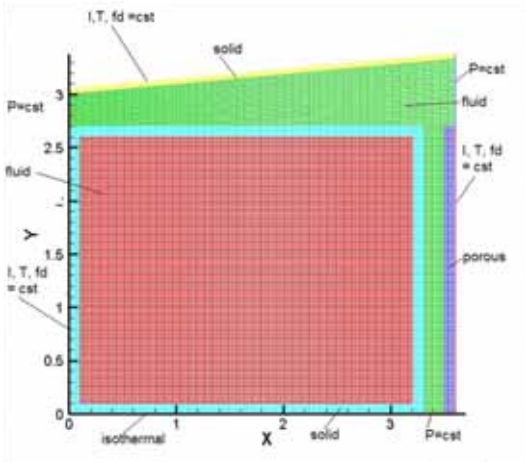

Fig. 3. Grid and Boundary conditions

5.2 Boundary conditions

The floor was assumed as a constant temperature wall, opaque which emits diffusively at an emissivity of ε = 0.92/0.72 depended on the wavelength band. For all the examined cases the floor temperature is set to T=293 K which is a simplifying approach.

In the North wall a mixed heat transfer boundary condition (combination of radiation and convection) is applied at the external boundary of the solid region. As far it concerns the radiation it is considered semi-transparent material where all the incident radiation is diffusive. A semi-transparent boundary condition implies that the incident radiation is reflected or transmitted by the surface. For that, the absorption coefficient of the adjacent solid zone is taken high enough to ensure that the whole transmitted radiation will be absorbed. This way the whole wall becomes opaque and the incident radiation is either reflected from the surface either absorbed, increasing the wall temperature. The heat transfer coefficient is taken h=7.1 W/mK.

The same boundary condition is imposed at the external surface of the shelter, where the heat transfer coefficient is set h=20 W/mK, and at the external south surface of the plants, where the heat transfer coefficient is set h=7.1 W/mK too. In the plants external surface the wall non-slip condition is substituted by a zero shear stress boundary condition. In this case the absorption coefficient of the adjacent porous material does not absorb all the transmitted incident radiation, but only a part of it.

All the internal walls are considered to be semi-transparent surfaces where the solid and fluid zones are coupled. This way the values of the variables are transferred from the one medium to the other. The trailing plants are considered as porous media with viscous resistance coefficient $\left(1/a\right) = 27380\,[m^{-2}]$, where a is the permeability and inertial resistance coefficient C_2= 1.534 [m^{-1}]. The porous material is coupled with the external boundary surface and the adjacent fluid. The equations of energy and radiations are also solved in all the solid and porous areas of the computational field. The flow both in the internal and the external fields is considered turbulent since the Ra number for the internal flow is 1.5×10^{10} and the Re number for the external flow is more than 1.9×10^{4}.

All the openings from where external air can enter or leave the computational field (right down opening between test cell and plants, right up opening between shelter and plants and left up opening between test cell and shelter) are considered as boundaries with constant pressure equal with atmospheric. The flow direction is determined by the whole field behavior as it is developed due to temperatures and the arising buoyancy forces. The air temperature in openings is set equal to the external air temperature.

When radiation reflected and transmitted from a specular semi-transparent surface, as it happens partly in our case, its direction is altered. The reflected radiation is given by

$$I_{W,a}\left(\vec{s}_r\right) = r_a\left(\vec{s}\right) I_{W,a}\left(\vec{s}\right) + \tau_b\left(\vec{s}'\right) I_{W,b}\left(\vec{s}_b\right) \tag{18}$$

Where, $I_{W,a}$ radiation intensity in the medium a, which is the air in our case, $I_{W,b}$ radiation intensity in the medium b, which is the solid, $\vec{s}$, direction of the incident radiation (from a to b), $\vec{s}_r$ direction of the reflected radiation, $\vec{s}'$, direction of the radiation incident to the surface from the solid side (from b to a), r_a, the interface air reflectivity and τ_b, the interface solid transmissivity. The radiation transmitted from the semi-transparent wall towards the solid is given by

$$I_{W,b}\left(\vec{s}_t\right) = r_b\left(\vec{s}'\right) I_{W,b}\left(\vec{s}\right) + \tau_a\left(\vec{s}'\right) I_{W,a}\left(\vec{s}_b\right) \tag{19}$$

Where, $\vec{s}$ is the direction of the refracted radiation inside the solid, r_b, the interface solid reflectivity and τ_a, the interface air transmissivity. The radiation directions are given by

$$\vec{s}' = \vec{s}_t - 2\left(\vec{s}\cdot\vec{n}\right)\vec{n} \tag{20}$$

Where, $\vec{n}$ is the normal to boundary unit vector, and

$$\vec{s}_r' = \vec{s} - 2\left(\vec{s}\cdot\vec{n}\right)\vec{n} \tag{21}$$

The interfaces' reflectivities and transmissivities are given by

$$r_a\left(\vec{s}\right) = \frac{1}{2}\left(\frac{n_a\cos\theta_b - n_b\cos\theta_a}{n_a\cos\theta_b + n_b\cos\theta_a}\right)^2 + \frac{1}{2}\left(\frac{n_a\cos\theta_a - n_b\cos\theta_b}{n_a\cos\theta_a + n_b\cos\theta_b}\right)^2 \tag{22}$$

$$\tau_b\left(\vec{s}'\right) = 1 - r_a\left(\vec{s}\right) \tag{23}$$

finally $r_b = r_a$ and $\tau_a = \tau_b$.

Where, n_a is the air refractive index, n_b the solid refractive index, θ_a the angle between the normal to the surface and the incident radiation direction $\vec{s}$ and θ_b, the angle between the normal to the surface and the refracted radiation direction inside the solid $\vec{s}_t$. It is obvious that in the case of unsteady calculations, those parameters should be calculated in every time step in each surface since the angle of incident radiation varies through the whole day.

$$\theta_b = \arcsin\left(\frac{n_a}{n_b}\sin\theta_a\right) \tag{24}$$

It should be noted that the above holds for $n_a < n_b$. The angle θ_a is given by (Duffie, J. A. & Beckman, W. A., 1991)

$$\cos\theta_a = \left(A - B\right)\sin\delta + \left[C\sin\omega + \left(D + E\right)\cos\omega\right]\cos\delta \tag{25}$$

$A = \sin\phi\cos\beta$, $B = \cos\phi\sin\beta\cos\gamma$, $C = \sin\beta\sin\gamma$, $D = \cos\phi\cos\beta$, $E = \sin\phi\sin\beta\cos\gamma$

Where, φ is the latitude (φ= 39º 38 in our case), δ is the declination, β is the surface slope, γ is the surface azimuth angle and ω is the hour angle. For the vertical south wall of plants it is

taken β=90° and γ=0°. For the shelter external surface it is taken β=5° and γ=180°. The angles δ and ω are given by

$$\delta = 23.45\sin\left(\frac{360(284+n)}{365}\right) \tag{26}$$

$$\omega = \left[(t_s + t) - 12\right]15 \tag{27}$$

Where, n is the day of the year, t_s and is the sunrise time.

5.3 Numerical details

The SIMPLEC (Patankar, S. V., 1980) algorithm is used for pressure-velocity coupling, yielding an elliptic differential equation in order to formulate the mass conservation equation. The discretisation of the convective terms in the Reynolds averaged transport equations is materialized by the QUICK scheme for the momentum equations, a second order upwind scheme (SOU) for the turbulence and radiation transport equations and by a third order MUSCL for the energy conservation equation. For the diffusive terms a central difference scheme is adopted. The convergence criterion was set to 10^{-4} for the continuity, momentum and turbulence equations while for energy the criterion was 10^{-8} and for radiation 10^{-6}. For the radiation model two wavelength bands are considered corresponding to solar spectrum (λ=0 -1.1 μm) and to thermal band (λ=1.1 – 100 μm).

6. Reference case

In order to validate the numerical model our study began with the simulation of a summer day for which experimental data about incident solar radiation, ambient temperature and temperatures developed inside the test cell infrastructure exists. For the validation it was chosen the simulation of 22nd of August of 2006 (Tzachanis A.D., 2008).

6.1 Experimental configuration

The experiments, used for validation, were carried out at the South-orientated façade of the test cell during a hot summer period (July to September) in Larissa, a Greek city with a climate characterized by long hot days in the summer. The measured data are presented in paper (Tzachanis, A.D, 2008). With a set of pyranometers with and with out shading rings were measured the diffuse irradiation, the beam irradiation and the global irradiation in a horizontal plane, as well as the global irradiation and the ground reflected irradiation in a vertical plane. The temperatures were also measured in the ambient, sunlit wall, shadowed wall and in the gap between the plants and the south wall by NiCr thermocouples.

6.2 Numerical configuration

The daily variations of incident irradiations and ambient temperature were approached with polynomials, in order to be used as boundary conditions in the simulation. The corresponding polynomials are given following

For the irradiation in vertical plane

$$I_v = -6.7 - 7.48x10^{-3}time + 6.21x10^{-6}time^2 - 2.38x10^{-10}time^3 + 2.33x10^{-15}time^4 \tag{28}$$

For the irradiation in horizontal plane

$$I_h = -1.74 + 6.28x10^{-3}\,time + 4.57x10^{-6}\,time^2 - 1.83x10^{-10}\,time^3 + 1.79x10^{-15}\,time^4 \quad (29)$$

For the ambient temperature

$$T_{amb} = 2.13 - 5.87x10^{-4}\,time + 2.29x10^{-7}\,time^2 - 1.72x10^{-11}\,time^3 + 5.97x10^{-16}\,time^4 - 1x10^{-20}\,time^5 + 6.43x10^{-26}\,time^6 \quad (30)$$

Where, *time* is the time since sunrise in secs. In both plane the percentage of diffuse irradiation f_d was 30%. Since there are not experimental measurements, it was supposed that the north wall received the half irradiation than the plants' vertical surface and that all of this irradiation was diffusive, f_d=1. In the 22nd of August in Larissa (φ=39.38°, L=22.25°) the solar sunrise time is 6h 39′ 36′′. Our simulation will begin from 6h 00′ 00′′ in the morning giving the opportunity to the flow field to reach a steady state condition, before the boundary conditions begin to alternate. The whole period of simulation is the total solar day from 6 h 00′ 00′′ up to 19h 20′ 00′′, a few minutes after the sunset. The time step is dτ=1 sec. The simulation results are saved every 60 secs.

6.3 Model validation

The numerical model was validated against the experimental measurements. Three temperatures were compared. The temperature developed in the gap between the plants and the shaded south wall, the temperature developed on the shaded south wall and the temperature developed on the sunlit surface. As simulated temperatures are considered the average temperatures: a) on a line across the gap in the elevation of 1.35 m for the gap temperature, b) on the surface of the south wall, for the shaded wall temperature, and c) in the surface on the sunlit shelter for the sunlit temperature. In the following figures 4, 5 and 6 the measured and simulated temperatures temporal profiles are given. The simulated temperatures are also compared with the temperatures calculated by steady-state simulations realized for the hours 8:00, 10:00, 12:00, 14:00, 16:00 and 18:00.

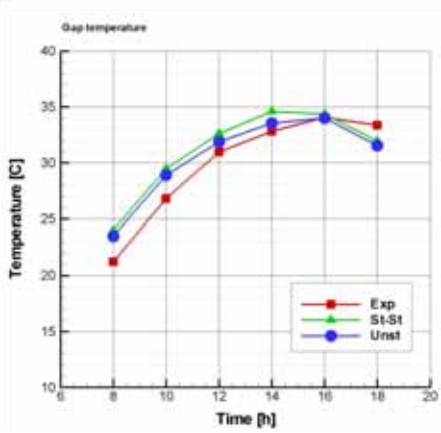

Fig. 4. Temporal profile of gap temperature

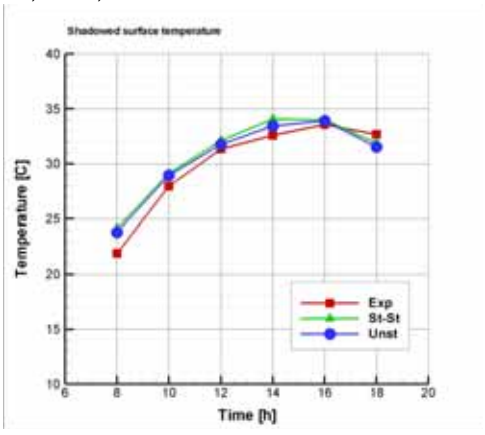

Fig. 5. Temporal profile of shadowed surface temperature

As far it concerns the gap and shaded surface temperatures we observe a fairly good approach with the unsteady simulation giving better results from the steady-state

simulation since it takes into account the phenomenon of thermal storage. The average deviation of unsteady simulation to the measured temperatures is of the order of 10%. Almost all the day the real temperatures are lower than the predicted. This is due to the fact that transpiration and the subsequent temperature decrease is not incorporated in the proposed model.

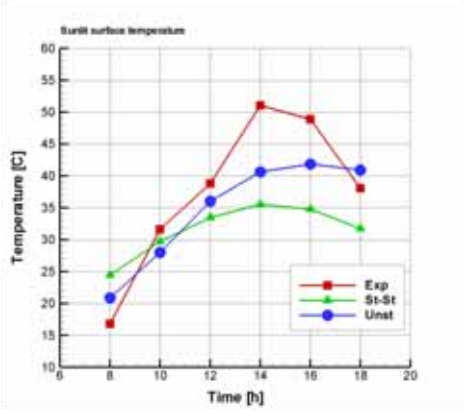

Fig. 6. Sunlit surface temporal temperature profile

As far it concerns the sunlit surface temperature profile we observe significantly more important improvement of temperature predictions passing from steady-state to unsteady radiation, in the order of 30% but the predicted values are still away from the measured especially for the hours between 14:00 and 16:00. As it has been pointed in the boundary conditions section a mixed boundary condition, taking account both convection and radiation, has been implemented to the shelter outer surface. Since the field around the shelter outer surface is not solved in this simulation a constant convection coefficient was adopted during all the day. It is likely at the afternoon hours the external wind speed to be enough low, so as to it led to a convection coefficient much lower than assumed. This could explain the deviation between measured and simulated temperatures during those hours.
In general the comparison is considered successful and the model is considered to simulate with fairly accuracy the transport phenomena takes part in the studied field. In following figures the most important flow and heat parameters in 6 characteristic hours are given in terms of iso-contours, streamlines and profiles. In fig.7 the temperature iso-contours inside the test cell are given for the hours 8:00, 10:00, 12:00, 14:00, 16:00 and 18:00.

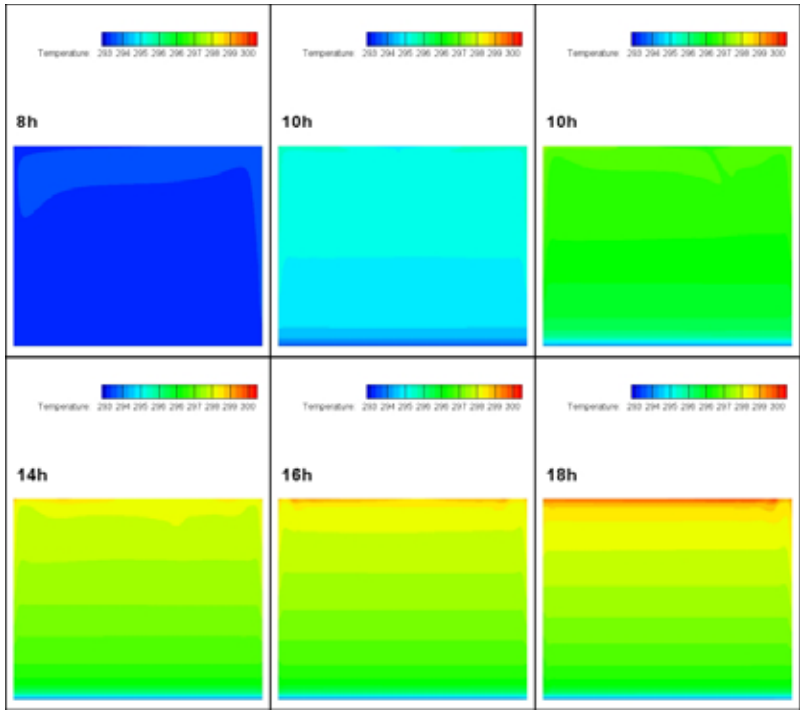

Fig. 7. Temperature iso-contours

During the day the temperature does not exceed the 27 °C, with the higher temperatures appearing at 18:00 h in the afternoon in the top of the cell. Although the north wall receives only diffusive radiation with the half intensity than the south the plants existence provide enough shadow to keep the south wall temperature low enough to cancel the appearance of any temperature gradient. The temperature in the floor remains 20 °C because it was selected to adopt the particular simplifying admission of isothermal boundary condition. In Fig.8 the temperature iso-contours around the test cell and between the cell and the shading devices are presented. In the external studied field the temperature can be as high as 36 °C, due to increased external air temperature and the heating through conduction, convection and irradiation. The higher temperature is observed in the 16:00 in the afternoon.

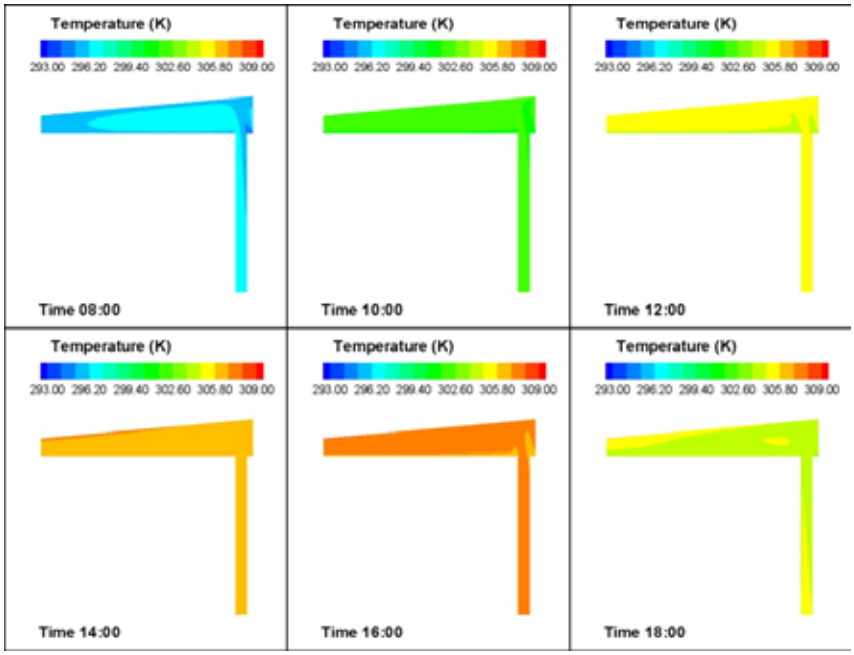

Fig. 8. Temperature iso-contours around the test cell

Finally in the figures 9 and 10 the temperature profiles along the x and y symmetry axes of the test cell are presented. The luck of any horizontal temperature gradient is verified. In the horizontal symmetry axis the temperature increase until 14:00 and then remains almost constant. The same behavior is observed along the vertical axis where the higher gradient appears during the afternoon.

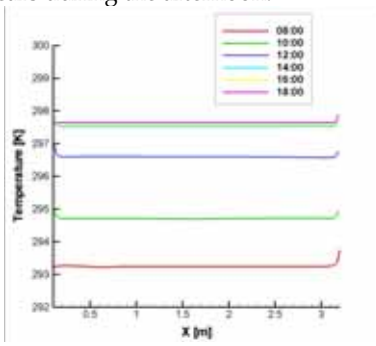

Fig. 9. Horizontal symmetry axis temperature profile

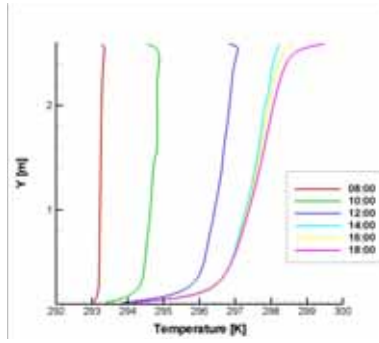

Fig. 10. Vertical symmetry axis temperature profile

In the figures 11 and 12 the streamlines and the isobaric contours are presented for the internal and the external field and the same hours.

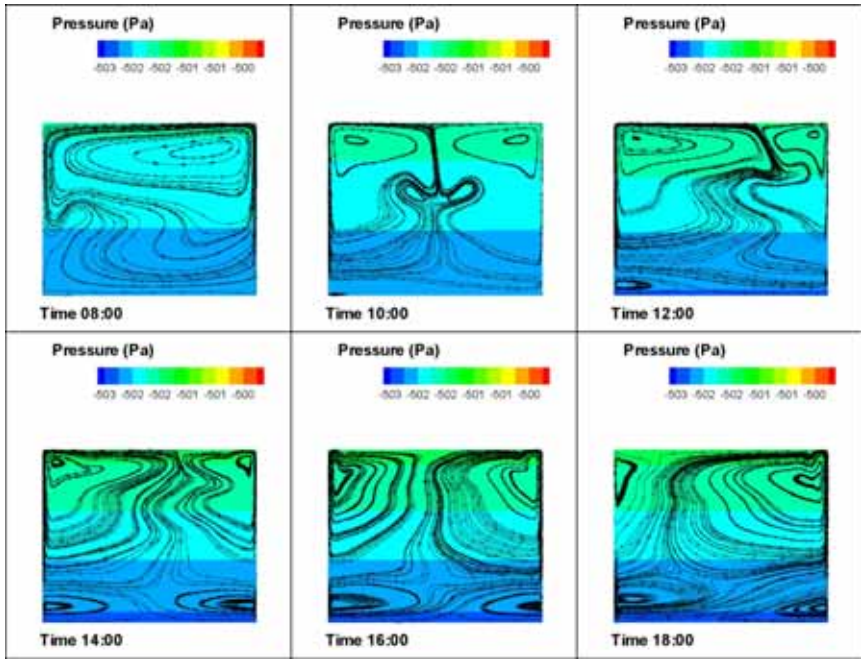

Fig. 11. Streamlines and isobaric contours inside the test cell

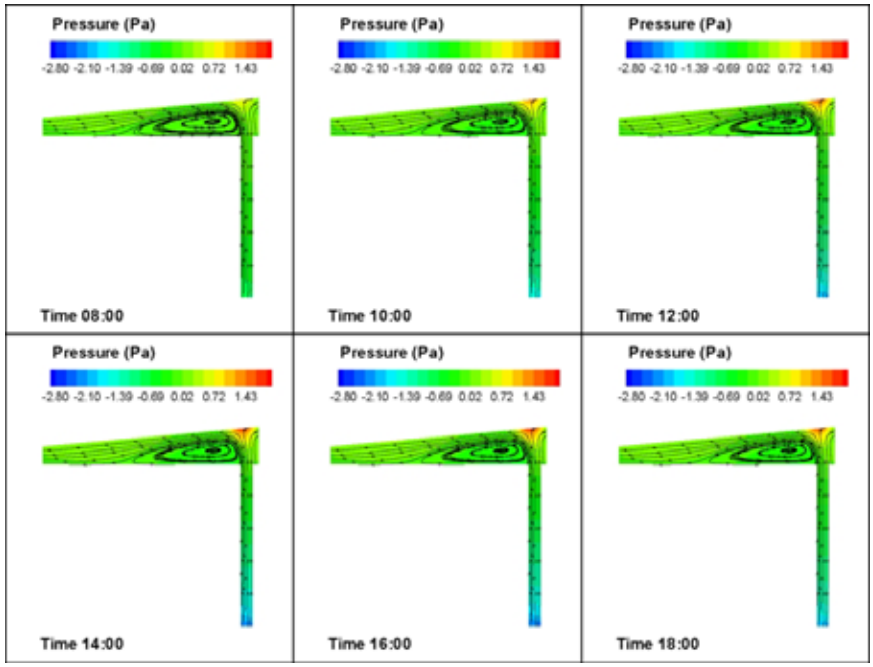

Fig. 12. Streamlines and isobaric contours outside the test cell

In both internal and external field the only driving force is the buoyancy. At the beginning of the day a unique big recirculation appears in the top left corner covering the whole internal field. Very soon it breaks in two recirculations sited in the top left and the top right corners, in the most heated areas of external walls. Other two smaller recirculations appears in the middle of the cell at 10:00, almost disappears at 12:00 and finally are established in the left and right bottom corners were they remains until the end of the day. From morning to the afternoon the left recirculation increases at the expense of the right one and then it decreases again as the ambient temperature, and consequently the north wall temperature, decreases. At the end of the day the right top recirculation is becoming dominant again. The external field flow pattern, between the test cell and the shading devices, remain almost unaltered as far it concerns the form. A solar chimney is developed between the plants and the south wall enforcing the external air to enter from the bottom and leave from the top openings, in the left between the test cell and the shelter and in the right between the shelter and the plants. The flow is separated in the cell left corner and reattached in the middle of the cell top forming and big recirculation. In the following figures 13, 14, 15 and 16 the u and v velocity components are given along the x and y symmetry axes inside the test cell.

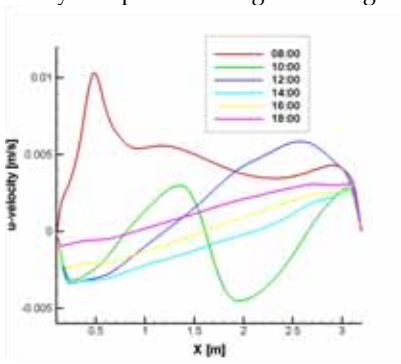

Fig. 13. u-velocity along x-symmetry axes

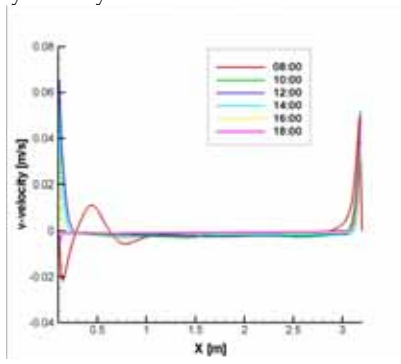

Fig. 14. v-velocity along x-symmetry axes

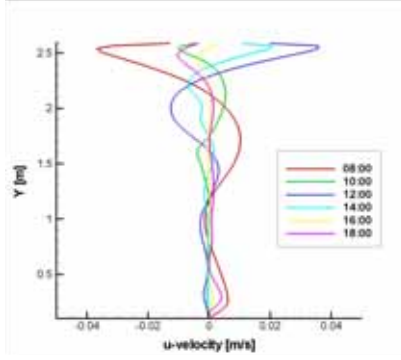

Fig. 15. u-velocity along y-symmetry axes

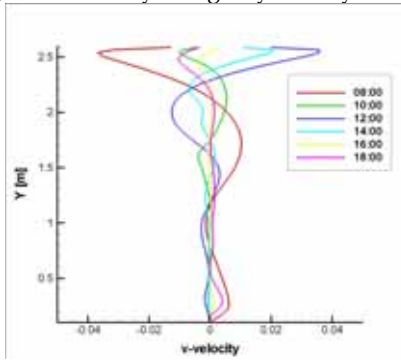

Fig. 16. v-velocity along y-symmetry axes

In all the cases velocities remains very low and don't exceed 0.08 m/s. Boundary layers seem to be well modeled. The v-velocity in horizontal axis remains almost zero except the areas close to the solid boundaries and almost time independent. In the vertical axis the most extreme behavior are observed for the hours 8:00 and 12:00, when the internal field is

altered until it reaches the almost steady afternoon condition. The same holds for the u component of velocity along the vertical axis. Along the horizontal axis u velocity component seems to undergo more severe alterations from morning to noon and it stabilizes during the afternoon.

In the figure 17 the iso-contours of the solar band incident radiation is presented. Plants prevent quite efficiently the entrance of solar radiation decreasing it up to 50%. The direct result is the reduction of the south wall temperature and consequently of the cooling loads. Finally in the figure 18 the Nusselt number profile in the shelter inner surface is given.

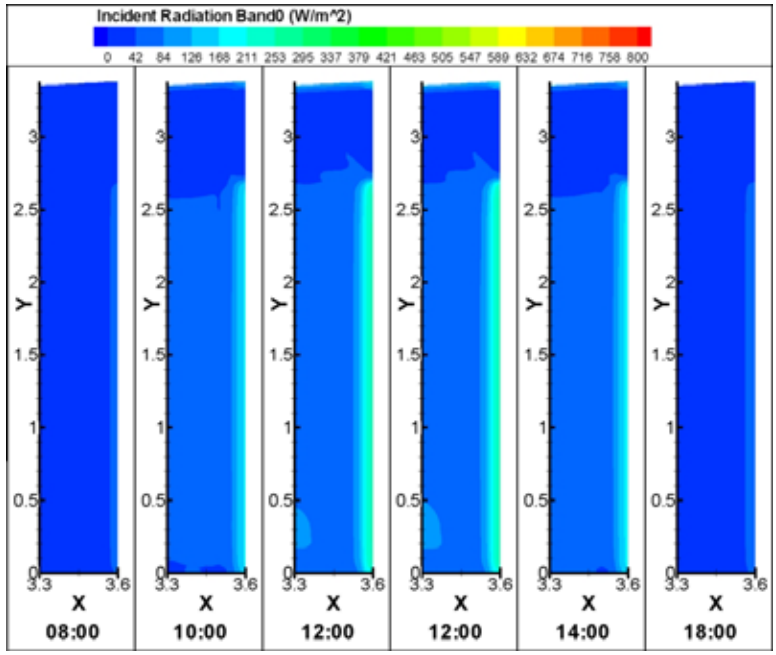

Fig. 17. Solar band of the incident radiation iso-contours

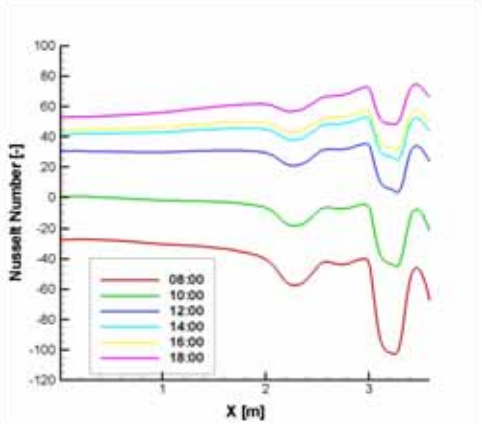

Fig. 18. Nusselt nuber profile in the shelter inner surface

In the site where the big recirculation appears a sudden drop of Nusselt number value occurs. Such a behavior would be impossible to be predicted with the usual semi-empirical analytical calculating tools based on the geometry and Re and Pr numbers. This figure reveals the CFD contribution in the common engineering problems since it allows the formulation a deep and accurate image of the real transport phenomena and a more precise estimation of the cooling loads and the gains arising from passive solar shading devices

7. Parametric study

The validated model was used for a parametric study in order to estimate the alteration of test cell mirco-climate due to the presence of plants during the whole summer. Four more characteristics days from May to September were simulated. Since there are not measured climatic data for those days, meteorological data available by CRES (Centre from Renewable Energy Sources of Greece) were used. In the Table 2 the monthly average daily radiation $\overline{H_{tot}}$ and the monthly average daily diffuse radiation $\overline{H_d}$ in horizontal plane are given. The 22nd day of each month is chosen as representative. In the same table the monthly average fraction of diffusive radiation $\overline{f_d}$ is given, along with the number of the day of the year, n.

Day	n [-]	$\overline{H_{tot}}$ [kWh/m²-d]	$\overline{H_d}$ [kWh/m²-d]	$\overline{f_d}$
22 May	142	6.66	1.97	0.30
22 June	173	7.13	2.00	0.28
22 July	203	7.74	1.82	0.24
22 September	265	4.94	1.44	0.29

Table 2. Radiation data for parametric study

From the above data it is calculated the monthly daily average beam irradiation in horizontal plane, $\overline{H_b}$ by the relation:

$$\overline{H_b} = \overline{H_{tot}} - \overline{H_d} \tag{31}$$

Taking into account the total duration of sunlight, NT, and assuming a sinusoidal variation we can calculate the beam normal irradiation $G_{b,nt}(\beta=0)$ [kW/m²] at any time of the day.

$$G_{b,nt}(\beta=0) = G_{b,n\max}(\beta=0)\sin\left[\frac{\pi \cdot time}{NT}\right] \tag{32}$$

Where, $G_{b,nmax}(\beta=0)$ is the maximum value of beam normal irradiation, in kW/m², given by

$$G_{b,n\max}(\beta=0) = \overline{H_b}\frac{\pi}{2NT} \tag{33}$$

The total number of sunlight hours, NT is calculated by

$$NT = \frac{2\omega_s}{15} \tag{34}$$

Where, ω_s, the sunrise hour angle given by

$$\omega_s = a\cos\left[-\tan\phi\tan\delta\right] \tag{35}$$

The total irradiation normal to the surface of sunlit test cell surfaces, $G_{tot,nt}(\beta)$ is given by

$$G_{tot,nt}(\beta) = \frac{G_{b,nt}(\beta)}{\overline{f_d}} \tag{36}$$

Where, $G_{b,nt}(\beta)$ the beam irradiation normal to the surface with inclination angle β given by

$$G_{b,nt}(\beta) = R_b G_{b,nt}(\beta=0) \tag{37}$$

In this relationship R_b is the ratio of beam irradiation on the plane to that on a horizontal surface at any time given by

$$R_b = \frac{\cos\theta_a}{\cos\theta_z} \tag{38}$$

Where, θ_z, is the zenith angle calculated by

$$\cos\theta_z = \sin j \sin\delta + \cos j \cos\omega \cos\delta \tag{39}$$

The irradiation in the plants surface is calculated with $\beta=90^o$ and $\gamma=0^o$, while the irradiation in the shelter with $\beta=5^o$ and $\gamma=180^o$. The irradiation on the north wall is taken half the irradiation on the plants and it is considered purely diffusive.

As far it concerns temperature it was assumed that it follows sinusoidal variation during the day under a rule of thumb

$$T(t) = a\sin(t) + b \tag{40}$$

$$t = \frac{time \cdot \pi}{NT} \text{ [hr]} \tag{41}$$

Where a and b are coefficients calculated from the minimum and maximum temperatures. The minimum and maximum temperatures have been retrieved from NASA meteorological site and are given in the table 3.

Table 3. Temperature for parametric study

Day	Minimum T [^{o}C]	Maximum T [^{o}C]	NT [h]	a [-]	b [-]
22 May	10.8	25.7	14.36	14.9	10.8
22 June	15.0	30.9	14.78	15.9	15.0
22 July	17.6	33.0	14.36	15.4	17.6
22 September	14.1	28.7	11.95	14.6	14.1

All the simulations covered the whole periods of sunlight. The time step used was $d\tau$= 2sec.

8. Results

In the figures 19 (a-e) the daily variation of characteristic average temperatures are given for the months May, June, July, August and September. Specifically in each figure are given the ambient temperature, the average room temperature, the average temperature in the gap between the south wall and the plants, the average temperature of the shaded south wall and the average temperature of the sunlit surface. The gap average temperature is the one taken in a line from the south wall to the porous plants at the elevation of 1.35 m. The picture is completed with fig. 19.f, the daily variation of ambient temperature imposed as external boundary condition for the five months. In all the cases the gap and the shaded surface temperatures are almost equal to the ambient temperature as it is imposed by the convection of the air stream entering the computational field from the bottom opening. The room temperature remains low enough and the sunlit temperature becomes far higher than the ambient one due to the solar radiation and the temporal heat storage. The highest ambient temperatures are found in July and August. In the figures 20 (a-e) the corresponding daily variations of average solar band radiation in the porous plants and in the gap are given, with the external solar band incident radiation in horizontal surface given

in fig. 20.f. In months close to the summer solstice very small amounts of solar band radiation are allowed to pass from the porous plants due to the incident angle and the optical properties. It should be noted that for the months May, June, July and September the percentage of ground reflected radiation and its direction was not taken into account.

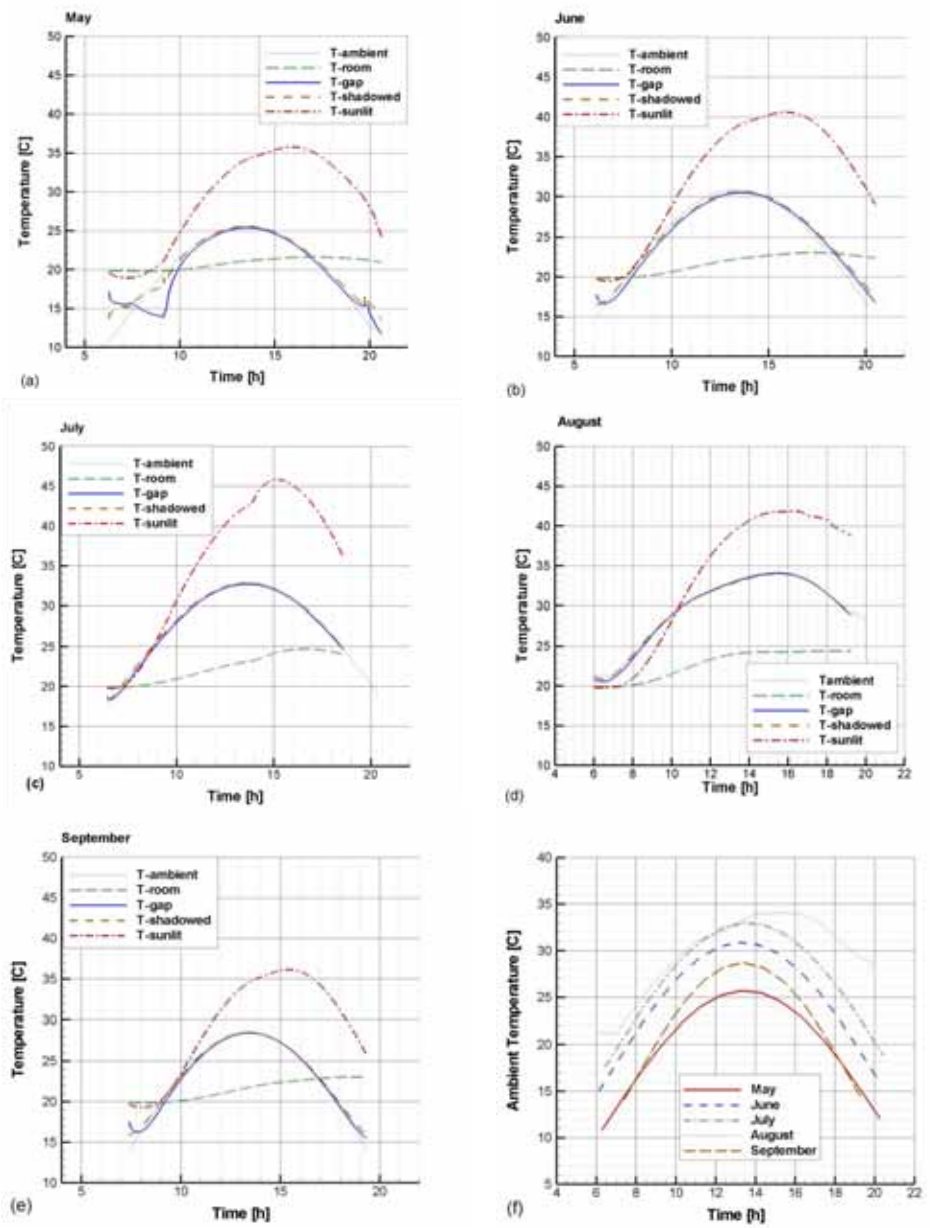

Fig. 19. Daily variation of average temperatures (a-e) and of ambient temperature (f)

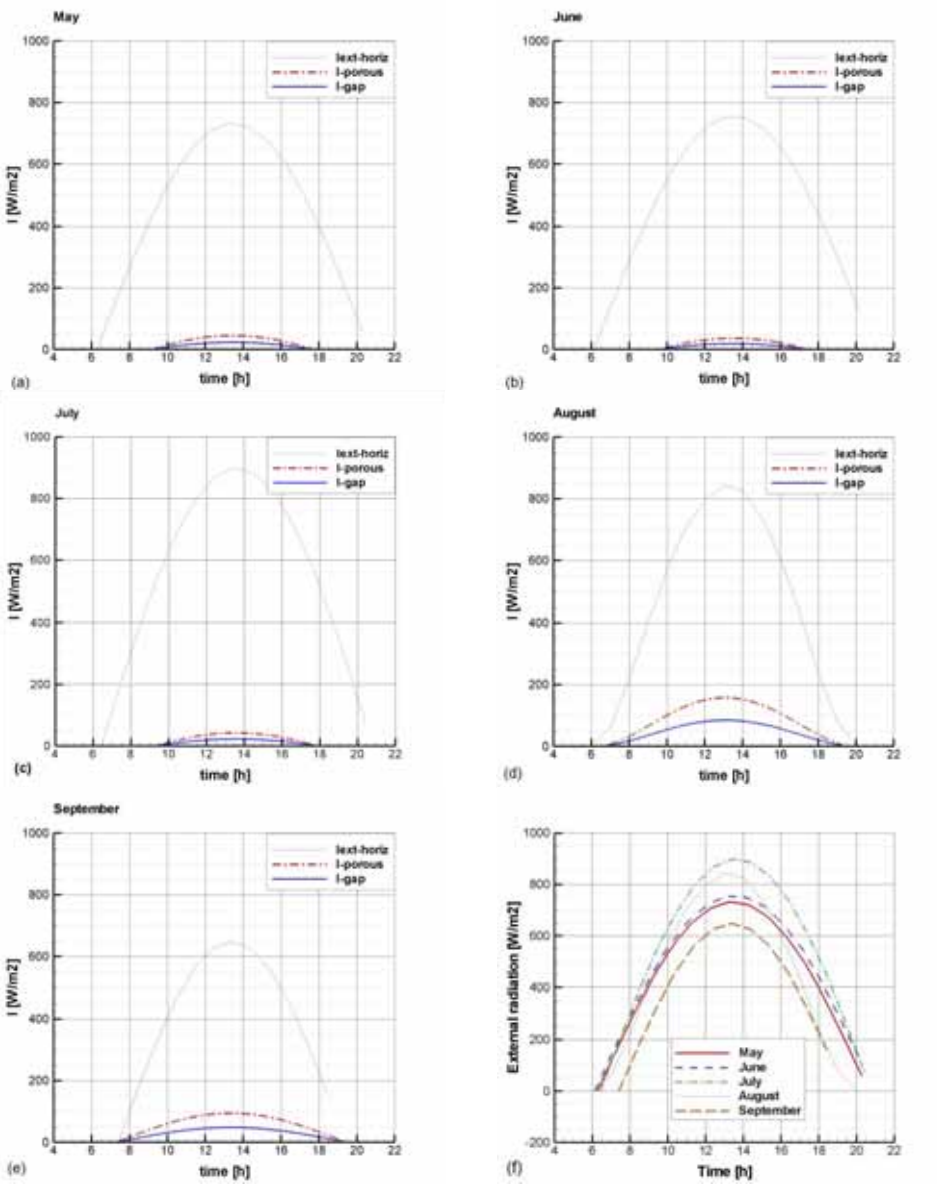

Fig. 20. Daily variation of average solar band radiation (a-e) and of external radiation incident on horizontal surface

In the figures 21 and 22, the daily variation of the average velocity magnitudes inside the room and in the gap between the plants and the south wall are given. The temperatures inside the room are very low as it was expected. They begin from relatively high values in the morning and the decrease stabilising for the rest of the day to very low values. This

behaviour is common to all months and agrees with the daily alteration of streamlines studied for August in Figure 11. In the gap it is observed that the higher the normal radiation in the plants external surface the higher the velocities in the created solar chimney.

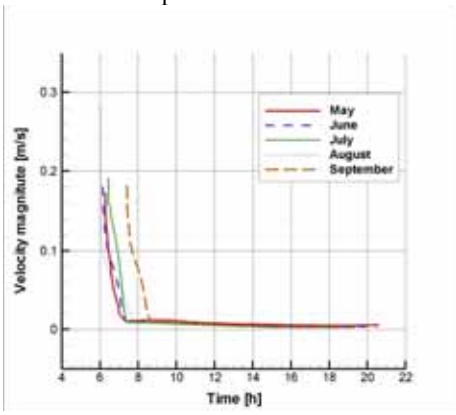

Fig. 21. Daily variation of room average velocities magnitude

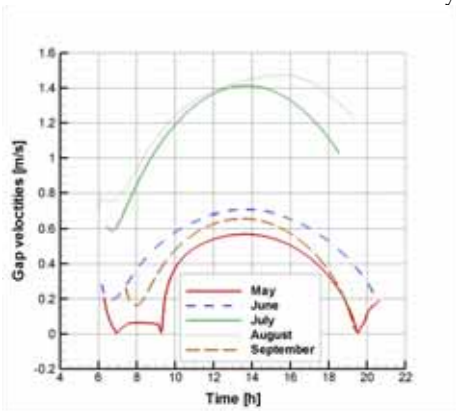

Fig. 22. Daily variation of gap average velocities magnitude

The basic goal of the plants use as passive solar shading devices is to decrease the cooling loads during the summer. Without the presence of the plants the south wall would have the sunlit surface temperature and energy should be consumed in order to remove the heat gain. This energy corresponds to the cooling load reduction achieved by the trailing pants presence. In the next figures 24 and 25 the daily variation of cooling load reduction and degree hours for the five examined months are presented. The degree hours (DH) and the cooling load reduction (CL) are calculated according to the following formulas

$$DH = (Tsunlit - Tshaded) * time \text{ [dh]} \tag{42}$$

$$CL = DH * area * surface\ heat\ transfer\ coefficient \text{ [Wh/m]} \tag{43}$$

Where the area is the south wall area per meter (*area* = 2.7 m²/m) and the *heat transfer coefficient* has been extracted from simulation results for the south wall surface.

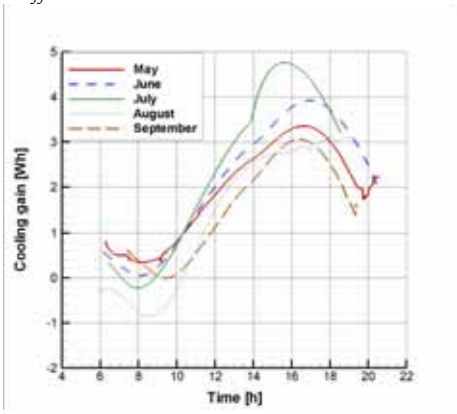

Fig. 23. Daily variation of cooling load reduction

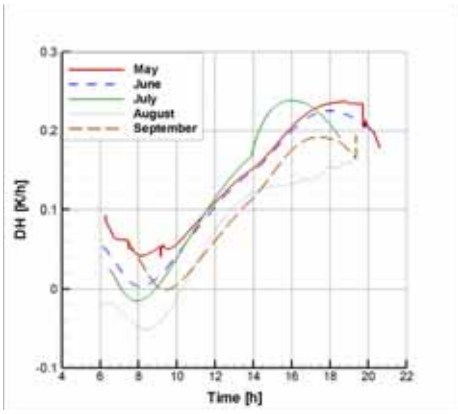

Fig. 24 Daily variation of degree hours

Integrating the cooling load reduction in the whole day time period the total daily energy saves can be calculated. In the Table 3 the energy saves per wall meter are summarized for the five examined months. August results agree with the energy saves calculated by experimentally measured data in (Tzachanis, A. D. 2008).

a/a	Month	Daily energy save [Wh/m]	Monthly energy save [kWh/m]
1	May	1651	51.81
2	June	1850	55.50
3	July	2038	63.18
4	August	1098	34.04
5	September	1127	33.81
		TOTAL	238.34

Table 3. Energy saving achieved by the trailing plants presence

9. Discussion

In the present work a CFD model was developed using a finite volume method for the simulation of flow and transport phenomena occurring in a test cell partially shaded by trailing plants and a shelter. The model was validated against obtained experimental measurements. It slightly overestimates the temperatures developed in the gap between the test cell south wall and the plant as well as the temperatures in the shaded south wall because it does not take into account the temperature reduction through transpiration. As far it concerns the temperature of sunlit surface a discrepancy is observed during some noon hours probably due to consideration of constant heat transfer coefficient as a boundary condition in the shelter external surface. Nevertheless the differences are small enough to consider the simulation successful and the model able to predict the developed flow, radiation and temperature patterns.

Inside the room the temperature during the whole day remains quite low due to thick insulation and the presence of the shading plants. The later is verified by the absence of horizontal temperature gradient although the north wall receives the half radiation of the south sunlit plants surface, which is also totally diffusive. The flow pattern inside the room alternates intensively during the first morning hours and it is stabilized in the afternoon hours. Between the test cell and the shading devices (trailing plants and shelter) a solar chimney is developed resulting in temperatures close to the ambient ones. In the whole computational field the only driving force is the thermal buoyancy. The time of maximum temperature is shifted towards the afternoon due to temporal heat storage phenomenon. The incident solar radiation is significantly reduced by the plants which are considered porous material with homogenous thermophysical and optical properties especially close the summer solstice when the incident angle increases.

The contribution of using CFD techniques for study of similar problems is revealed from the Nusselt number profile on the shelter inner surface, indicatively given in the figure 18, which would be impossible to be predicted with analytical semi-empirical tools.

The parametric study allows the calculation of cooling load reduction, offered by the presence of plants in the south wall vicinity, during the whole period of high ambient temperatures of the year. It shows considerable reduction of cooling loads which could lead

to important energy save during a period with high power demand. The quantification of this energy save was the basic object of the simulation realised in this work.

10. Conclusion – Suggestion

The placing of plants near the south walls offer important reduction in buildings cooling loads, as it is known from traditional architecture and bioclimatic design principles. In the present work their effect was simulated using Computational Fluid Dynamic (CFD) techniques allowing the quantification of energy saving during the hot summer period. The developed model is considered successful since it compares well with existing experimental measurements.

Nevertheless the model can be improved further. One important step is the introduction of the mechanism of temperature reduction due to the plants transpiration that could allow better estimation of temperatures fields. Another step could be the 3D simulation that would allow more accurate calculation of the expected energy saving.

A better approach of the boundary condition imposed on the test cell ground would give a more realistic estimation of the flow and temperature pattern developed inside the test cell, allowing the extraction of conclusion about the comfort conditions there.

One important parameter is the value of the thermophysical and spectral optical properties of the involved materials. Especially as far it concerns the plant it would be very useful to measure accurately the optical properties and use them in a more appropriate wavelength band discretization. The model can be used for the evaluation of different plants performance and it can allow the design of effective passive solar shading systems.

11. References

Achard, P. & Gicquel, R. (1986). *European Passive Solar Handbook:Basic principles and concepts for passive solar architecture,* Commission of the European Communities, Directorate-General XII for Science, Research and Development (Brussels)

Akbari, H., Kurn, D. M., Bretz, S. E. & Hanford, J. W. (1997). Peak power and cooling energy savings of shade trees, *Energy and Buildings,* 25(2), *pp*. 139-148

Ali-Toudert, F. & Mayer, H. (2007). Effects of asymmetry, galleries, overhanging facades and vegetation on thermal comfort in urban street canyons, *Solar Energy,* 81(6), *pp*. 742-754

Baxevanou, C. A., Fidaros, D. K. & Tzachanis, A. D. (2008). *Plant's shading effect in a test cell - A CFD study*. Applied Simulation and Modelling, Corfu, Greece, Acta Press.

Carter, C. & De Villiers, J. (1987). *Principles of passive solar building design: with microcomputer programs,* 0080336361, New York.

Chui, E. H. & Raithby, G. D. (1993). Computation of radiant heat transfer on a nonorthogonal mesh using the finite-volume method, *Numerical Heat Transfer, Part B: Fundamentals,* 23(3), *pp*. 269-288

Duffie, J. A. & Beckman, W. A. (1991). *Solar engineering of thermal processes,* Wiley, 0471510564, New Jersey.

Erell, E. & T. Williamson (2006). Simulating air temperature in an urban street canyon in all weather conditions using measured data at a reference meteorological station, *International Journal of Climatology,* 26(12), *pp*. 1671-1694

Ferziger, J. H. & Perić, M. (2002). *Computational Methods for Fluid Dynamics,* Springer, 3540420746, Berlin.

Gan, G. (2006). Simulation of buoyancy-induced flow in open cavities for natural ventilation, *Energy and Buildings,* 38(5), *pp*. 410-420

Goulding, J. R., Lewis, J. O. & Steemers, T. C. (1992). *Energy Conscious Design: A Primer for European Architects,* BT Batsford Ltd., London.

Goulding, J. R., Lewis, J. O. & Steemers, T. C. (1993). *Energy In Architecture The European Passive Solar Handbook,* Batsford for the Commission of the European Communities, 0713469188

Kim, S. H. & Huh, K. Y. (2000). A new angular discretization scheme of the finite volume method for 3-D radiative heat transfer in absorbing, emitting and anisotropically scattering media, *International Journal of Heat and Mass Transfer,* 43(7), *pp*. 1233-1242

Launder, B. E. & Spalding, D. B. (1974). The numerical computation of turbulent flows, *Computer Methods in Applied Mechanics and Engineering,* 3(2), *pp*. 269-289

Liu, Y. & Harris, D. J. (2008). Effects of shelterbelt trees on reducing heating-energy consumption of office buildings in Scotland, *Applied Energy,* 85(2-3), *pp*. 115-127

Miyazaki, T., Akisawa, A. & Kashiwagi, T. (2006). The effects of solar chimneys on thermal load mitigation of office buildings under the Japanese climate, *Renewable Energy,* 31(7), *pp*. 987-1010

Mochida, A., Yoshino, H., Miyauchi, S. & Mitamura, T. (2006). Total analysis of cooling effects of cross-ventilation affected by microclimate around a building, *Solar Energy,* 80(4), *pp*. 371-382

Modest, M. F. (2003). *Radiative Heat Transfer,* Academic Press, 0125031637.

Papadakis, G., Tsamis, P. & Kyritsis, S. (2001). An experimental investigation of the effect of shading with plants for solar control of buildings, *Energy and Buildings,* 33(8), *pp*. 831-836

Patankar, S. V. (1980). *Numerical heat transfer and fluid flow,* Taylor & Francis, 0891165223, Hemisphere.

Raeissi, S. & Taheri, M. (1999). Energy saving by proper tree plantation, *Building and Environment,* 34(5), *pp*. 565-570

Raithby, G. D. (1999). Discussion of the finite-volume method for radiation, and its application using 3D unstructured meshes, *Numerical Heat Transfer, Part B: Fundamentals,* 35(4), *pp*. 389-405

Raithby, G. D. & Chui, E. H. (1990). Finite-volume method for predicting a radiant heat transfer in enclosures with participating media, *Journal of Heat Transfer,* 112(2), *pp*. 415-423

Tzachanis, A. D. (2008). The contribution of natural shading with climbing plants to the energy balance of a building, *Geotechnical Scientific Topics of GOETEE,* In press*pp*.

Tzachanis, A. D. & Sdravopoulou, C. (2002). *Simulation on the periodic steady heat gain in buildings*. 2nd IASTED International Conference on Power & Enrgy Systems (Euro PES), Crete, Greece.

Wilcox, D. C. (1998). *Turbulence Modeling for CFD,* DCW Industries, 0963605151, California.

Zhang, Y., Mahrer, Y. & Margolin, M. (1997). Predicting the microclimate inside a greenhouse: an application of a one-dimensional numerical model in an unheated greenhouse, *Agricultural and Forest Meteorology,* 86(3-4), *pp*. 291-297